Mechanism of the Conformational Transitions in 6-Hydroxymethyl-7,8-dihydropterin Pyrophosphokinase as Revealed by NMR Spectroscopy†,‡

Guangyu Li,§ Krzysztof Felczak,|| Genbin Shi,⊥ and Honggao Yan*

Department of Biochemistry and Molecular Biology, Michigan State University, East Lansing, Michigan 48824

Received May 27, 2006; Revised Manuscript Received August 17, 2006

ABSTRACT: 6-Hydroxymethyl-7,8-dihydropterin pyrophosphokinase (HPPK) catalyzes the transfer of pyrophosphate from ATP to 6-hydroxymethyl-7,8-dihydropterin (HP), leading to the biosynthesis of folate cofactors. HPPK undergoes dramatic conformational changes during its catalytic cycle, and the conformational changes are essential for enzymatic catalysis. Thus, the enzyme is not only an attractive target for developing antimicrobial agents but also an excellent model system for studying the catalytic mechanism of enzymatic pyrophosphoryl transfer as well as the role of protein dynamics in enzymatic catalysis. In the present study, we report the NMR solution structures of the binary complex HPPK•MgAMPCPP and the ternary complex HPPK•MgAMPCPP•DMHP, where α,*β*-methyleneadenosine triphosphate (AMPCPP) and 7, 7-dimethyl-6-hydroxypterin (DMHP) are the analogues of the substrates ATP and HP, respectively. The results suggest that the three catalytic loops of the binary complex of HPPK can assume multiple conformations in slow exchanges as evidenced by multiple sets of NMR signals for several residues in loops 2 and 3 and the very weak or missing NH cross-peaks for several residues in loops 1 and 3. However, the ternary complex shows only one set of NMR signals, and the cross-peak intensities are rather uniform, suggesting that the binding of the second substrate shifts the multiple conformations of the binary complex to an apparently single conformation of the ternary complex. The NMR behaviors and conformations of the binary complex HPPK•MgAMPCPP are significantly different from those of HPPK in complex with Mg*β*,*γ*-methyleneadenosine triphosphate (MgAMPPCP). It is suggested that the conformational properties of the binary substrate complex HPPK•MgATP be represented by those of HPPK•MgAMPCPP, because MgAMPCPP is a better MgATP analogue for HPPK with respect to both binding affinity and bound conformation.

6-Hydroxymethyl-7,8-dihydropterin pyrophosphokinase (HPPK[1]) catalyzes the transfer of pyrophosphate from ATP to 6-hydroxymethyl-7,8-dihydropterin (HP, Figure 1), leading to the biosynthesis of folate cofactors (*1*). Folate cofactors are essential for life (*2*). Mammals have an active transport system for deriving folates from their diets. In contrast, most microorganisms must synthesize folates *de novo*, because they lack the active transport system. Therefore, like other enzymes in the folate biosynthetic pathway, HPPK is an attractive target for developing antimicrobial agents. *E. coli* HPPK is also an excellent model system for studying the catalytic mechanism of enzymatic pyrophosphoryl transfer and has emerged as an excellent model system for studying the role of protein dynamics in enzymatic catalysis because

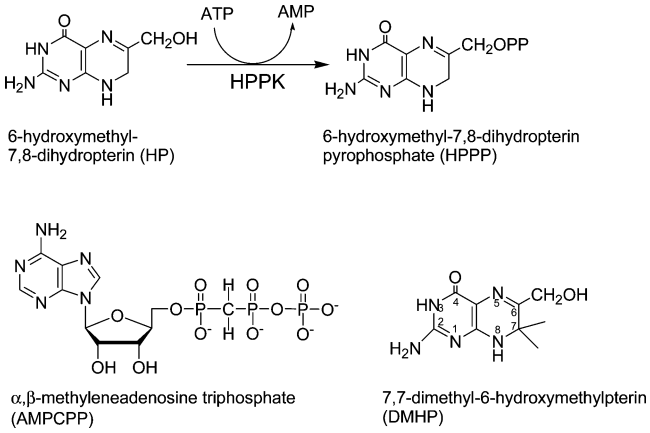

FIGURE 1: HPPK catalyzed reaction and the chemical structures of the substrate analogues.

† This work was supported in part by NIH Grant GM51901 (to H.Y.). This study made use of a Varian INOVA-600 NMR spectrometer at Michigan State University funded in part by NSF Grant BIR9512253.

‡ The coordinates of the refined solution structures of the binary complex HPPK•MgAMPCPP and the ternary complex HPPK•MgAMPCPP•DMHP have been deposited with the Protein Data Bank, and the accession codes are 2F65 and 2F63, respectively.

⊥ Current address: Division of Nephrology, Vanderbilt University School of Medicine, S3223 Medical Center, North 21st Street South, Nashville, TN 37232.Fax: 517-353-9334. E-mail: yanh@msu.edu.

§ Current address: NMR Research Facility, College of Basic Sciences, Louisiana State University, Baton Rouge, LA 70803.

|| Current address: Center for Drug Design, University of Minnesota, 516 Delaware Street, S. E., Minneapolis, MN 55455.

* To whom correspondence should be addressed. Tel: 517-353-5282. Fax: 517-353-9334. E-mail: yanh@msu.edu.

[1] Abbreviations: AMPCPP, α,*β*-methyleneadenosine triphosphate; AMPPCP, *β*,*γ*-methyleneadenosine triphosphate; DMHP, 7,7-dimethyl-6-hydroxymethylpterin; HP, 6-hydroxymethyl-7,8-dihydropterin; HPPK, 6-hydroxymethyl-7,8-dihydropterin pyrophosphokinase; HSQC, heteronuclear single-quantum coherence; NOE, nuclear Overhauser effect.

10.1021/bi061057m CCC: $33.50
Published on Web 09/20/2006

the enzyme is small (~18 kDa), stable, and amenable to both X-ray crystallographic and NMR analysis.

Comparative analysis of the crystal structures of ligand-free HPPK and its ternary complex has revealed that the complete active center of HPPK is assembled only after both substrates bind to the enzyme (*3*). The assembling of the active center involves large conformational changes, particularly in three catalytic loops. Of the three catalytic loops, loop 3 undergoes the most dramatic conformational changes. As expected, the loop moves in to close the active center upon the formation of the ternary complex (*3*). However, the loop moves away from the active center upon the binding of MgADP or the MgATP analogue Mgβ,γ-methyleneadenosine triphosphate (MgAMPPCP) (*4*). Recently, it has been shown that loop 3 also moves away from the active center upon the completion of pyrophosphoryl transfer, to the same extent as that upon the binding of MgADP or MgAMPPCP (*5*). By site-directed mutagenesis, it has been shown that loop 3 is required for the assembling of the full active center, plays an important role in the stabilization of the ternary complex and the transition state of the reaction, and is essential for catalysis (*6*, *7*). The dramatic conformational changes during the catalytic cycle of HPPK as revealed by these structures can be described by an induced fit model. However, NMR analysis suggested that the three catalytic loops of the apo HPPK undergo conformational exchanges because the backbone resonances of many residues in these loops show no cross-peaks or very weak ones (*8*). A more recent molecular dynamics simulation study also suggested that a population shift model is more appropriate for the conformational transitions associated with ligand binding in HPPK (*9*).

The HPPK-catalyzed reaction follows an ordered kinetic mechanism with ATP binding to the enzyme first (*10*, *11*). Atomic structures have been determined for nearly every stage of the catalytic cycle (*3*−*5*, 12−14). Currently, representing the binary complex with the substrate ATP is the NMR solution structure of the binary complex with Mgβ,γ-methyleneadenosine triphosphate (MgAMPPCP), with loop 3 assuming an unusually open conformation (pdb code: 2F65) (*4*). MgAMPPCP was used for the NMR study because MgATP can be hydrolyzed to MgADP in the presence of HPPK (*4*). However, subsequent biochemical and structural studies indicated that Mgα,β-methyleneadenosine triphosphate (MgAMPCPP) is a better analogue for MgATP for HPPK with respect to both binding affinity and bound conformation (*3*, *11*, *14*).

In this article, we report the NMR solution structures of the binary complex of HPPK with the MgATP analogue MgAMPCPP and the ternary complex with MgAMPCPP and the HP analogue 7,7-dimethyl-6-hydroxymethylpterin (DMHP; see Figure 1 for its chemical structure). The results indicate that in the binary complex HPPK•MgAMPCPP, loops 2 and 3 can assume multiple conformations in slow exchange on the NMR chemical shift time scale as evidenced by multiple sets of NMR signals. The loop conformations of the major species of the binary complex HPPK•MgAMPCPP are significantly different from those of HPPK in complex with MgAMPPCP. In the ternary complex HPPK•MgAMPCPP•DMHP, these loops assume an apparently single conformation. Thus, the NMR studies suggest that the conformational transitions from the apo enzyme to the ternary substrate complex during the catalytic cycle of HPPK are not simply from one conformation to another but involve multiple conformational equilibria.

EXPERIMENTAL PROCEDURES

Synthesis of DMHP. DMHP (Figure 1 and **8** in Scheme 1 in the Supporting Information) was synthesized by a modified procedure of Wood and Stuart (*15*). The original Wood and Stuart procedure was based on a classical method for the preparation of 7,8-dihydropteridines (*16*), condensation of α-aminoketone with halopyrimidinone followed by reductive cyclization. DMHP was prepared by the condensation of 2-amino-5-nitro-6-chloropyrimidin-4-one (**4**) with 3-amino-1-hydroxy-3-methyl-butan-2-one under basic conditions. The synthesis of the key α-aminoketone was troublesome, however, and a number of modifications of this strategy were developed (*17*). Because the pyrimidine component is not stable and easily undergoes hydrolysis, in our modified procedure, it was synthesized by direct nitration of commercial 2-amino-6-chloropyrimidin-4-one according to a recent method by De Jong and co-workers and their finding that converting it into ammonium salt significantly increases the stability of this compound (*18*). We observed that the ethyldiisopropylammonium salt of **4** provides the best result in the condensation. The aminoketone component (**3**) was prepared by starting from 3,3-dimethylallyl alcohol (**1**) with the addition of *in situ* generated nitrosyl chloride from isoamyl nitrite and HCl followed by aminolysis. Condensation of **3** with the ethyldiisopropylammonium salt of **4** was catalyzed by *N*-methylmorpholine as a base. Sodium dithionite-promoted reductive cyclization resulted in the formation of DMHP (**8**). All analytical data (UV absorption, NMR, and mass spectrometry) are in agreement with those previously reported.

Sample Preparation. AMPCPP was purchased from Sigma. HPPK was isotopically labeled and purified as previously described (*8*). The NMR samples were dissolved in a buffer made with 95% H_2O/5% D_2O. The buffer contained 20 mM sodium phosphate, 15 mM $MgCl_2$, and 50 μM 2,2-dimethyl-2-silapentane-5-sulfonate (as an internal chemical shift standard) at pH 7.4 (pH meter reading). Both the binary and ternary complex samples contained 1.6 mM HPPK and 10 mM AMPCPP; the ternary complex sample also contained ~2.1 mM DMHP, sufficient for saturating the enzyme. The ^{15}N,^{13}C-labeled samples were placed in Shigemi microcells.

NMR Spectroscopy. All NMR data were recorded on a Varian 600 MHz INOVA spectrometer at 25 °C. The NMR data were processed using NMRPipe (*19*) and the spectra analyzed using NMRView (*20*). The sequential backbone and C^β resonance assignments were made from a combined analysis of the HNCACB and CBCA(CO)NH spectra. The assignments of the binary complex were also confirmed by the ^1H-^{15}N HSQC spectra of the protein samples labeled with ^{15}N-Ala, Gly/Ser, Leu, or Val. Side-chain proton and carbon chemical shift assignments were made from the combined analysis of HCCH-TOCSY, H(CCO)NH-TOCSY and (H)C(CO)NH-TOCSY spectra, and aided and confirmed by the analysis of NOEs from 3D ^{15}N- and ^{13}C-edited NOESY spectra. The protons of the aromatic side chains were achieved by the analysis of NOEs from 3D ^{13}C-edited NOESY spectra. {^1H}-^{15}N Heteronuclear NOEs were mea-

sured from an interleaved pair of 2D ^{15}N-^{1}H gradient sensitivity enhanced correlation spectra with and without 3 s proton saturation (*21*). The recycle delay for the NOE experiments was 5 s.

Structure Calculation. The programs ARIA (version 1.2) (*22*−*24*) and CNS (version 1.0) (*25*) were used to compute the solution structures. The restraints used to calculate structures included dihedral angles and NOEs. Dihedral angle restraints were derived from secondary chemical shifts using the program TALOS (*26*). All NOE cross-peaks from 3D ^{15}N- and ^{13}C-edited NOESY spectra and chemical shift assignments were used as inputs for ARIA, and as many artifact peaks as possible were deleted manually. The NOE peak lists were unassigned and not calibrated with respect to distance.

For the ternary complex, a global fold was obtained from an extended structure with random side-chain conformations based on the aforementioned dihedral angles, chemical shift assignments, and NOE peak lists, but the convergence of the structures was poor. The global fold was similar to that of the previously reported crystallographic structure. Therefore, the crystal structure was used as the template structure for ARIA to make NOE assignments. The unambiguously assigned restraints obtained from ARIA, together with the previously obtained NMR restraints, were then used for a new round of ARIA calculations. This algorism was successful, and an ensemble of well converged structures were obtained. A similar strategy was used for the structure calculation of the binary complex with additional hydrogen bond restraints. The hydrogen bond restraints were derived from the secondary chemical shift analysis using the program TALOS (*26*) and manually assigned NOEs. In total, 47 hydrogen bonds were assigned, 16 in β-sheets and 31 in α-helices. With these additional hydrogen bond restraints, an ensemble of well converged structures was obtained. In the final round, 100 structures, instead of the ARIA default of 7, were calculated, and 20 structures with lowest energies and minimal NOE violations were selected and further refined by a short simulated annealing run with an explicit water shell.

RESULTS

NMR Analysis of the Binary Complex HPPK•MgAMPCPP

Resonance Assignment and Conformational Heterogeneity. As mentioned earlier, the HPPK-catalyzed pyrophosphoryl transfer reaction follows an ordered kinetic mechanism. The first complex in the catalytic cycle is formed by HPPK and MgATP. However, the binary substrate complex is not stable enough for prolonged NMR experiments because the enzyme has a low level of ATPase activity, and the bound ATP can be hydrolyzed to ADP (*4*). However, MgAMPCPP is an excellent MgATP analogue for HPPK on the basis of biochemical and structural studies (*3*, *11*, *14*). The sequential resonance assignment of the binary complex HPPK•MgAMPCPP was achieved by the concerted analysis of a set of double and triple resonance NMR spectra and the HSQC spectra of the binary complex of four selectively ^{15}N-labeled proteins as described in the Experimental Procedures section.

All expected backbone amide resonances were assigned, except those of residues T1, S13, E16, R82, W89, G90, and L94, which were missing. Great efforts were made to assign as many side-chain resonances as possible, particularly for those residues with missing or weak amide resonances. For example, the cross-peak of E80 was missing in the ^{1}H-^{15}N HSQC spectrum, but its side chain proton and carbon resonances could be assigned by the combined analysis of HNCACB, CBCA(CO)NH, and HCCH-TOCSY spectra. For P91, because it has no NH group and the NH group of the following residue R92 showed a very weak cross-peak, its $C^{\alpha}C^{\beta}$ chemical shifts could not be identified directly, but the side chain resonances of P91 could still be assigned by comparison with the resonance assignment of the ternary complex HPPK•MgAMPCPP•DMHP, to be described later. In the end, only four residues remained without any resonance assignment: S13 in loop 1 and R82, W89, and G90 in loop 3. The nearly complete sequential assignment provided a solid foundation for using ARIA to calculate the structure of the binary complex HPPK•MgAMPCPP, which mostly relies on the completeness and accuracy of the resonance assignment.

A significant finding of the sequential assignment was that most residues in loop 2 showed two sets of NMR signals, a major and a minor cross-peak corresponding to a major and a minor conformation, respectively, as illustrated in Figures 2 and 3. Figure 2 shows the two sets of sequential connectivities for residues P44 to Q50. Figure 3 shows the two cross-peaks for G46 in the HSQC spectrum of the binary complex of HPPK selectively labeled with ^{15}N-glycine/serine. Of the six serine residues in HPPK, S9 in loop 1 had a very weak cross-peak, and S13, also in loop 1, had no cross-peak, whereas four other serine residues had cross-peaks of normal intensities. Of the eight glycine residues, G46 in loop 2 had two cross-peaks labeled G46 and G46′, and G90 in loop 3 had no cross-peak, whereas the other six glycine residues showed cross-peaks of normal intensities. The intensity ratio of the major and minor cross-peaks was about 10:1 for G46 but dropped to 4:1 for D49, suggesting that loop 2 might assume more than two sets of conformations in slow exchange on the NMR chemical shift time scale, which is determined by the rate of conformational exchange relative to the chemical shift difference. Two sets of NMR signals were also observed for A86 and E87 in loop 3 (Figure S1). That these residues had two sets of NMR signals indicated that loop 3 in the binary complex also has at least two conformations. Conformational exchanges were probably the cause of missing or very weak cross-peaks for the loop 3 residues E80, R82, V83, R88, W89, G90, R92, and L94 in the ^{1}H-^{15}N HSQC spectrum. No multiple sets of NMR signals were observed for the residues in loop 1, which is coupled to both loops 2 and 3 (*3*). However, residues S9−A12 showed only very weak cross-peaks, and S13 had no cross-peak in the ^{1}H-^{15}N HSQC spectrum, suggesting that loop 1 also undergoes a conformational exchange.

Structure Determination. The solution structure of the binary complex HPPK•MgAMPCPP was calculated using ARIA (*22*, *23*) with an input file containing chemical shift assignments, NOE peak lists, dihedral angles, and hydrogen bond restraints. For residues with multiple sets of NMR signals, only the major NMR signals were used for the structure calculation. A total of 100 structures were calcu-

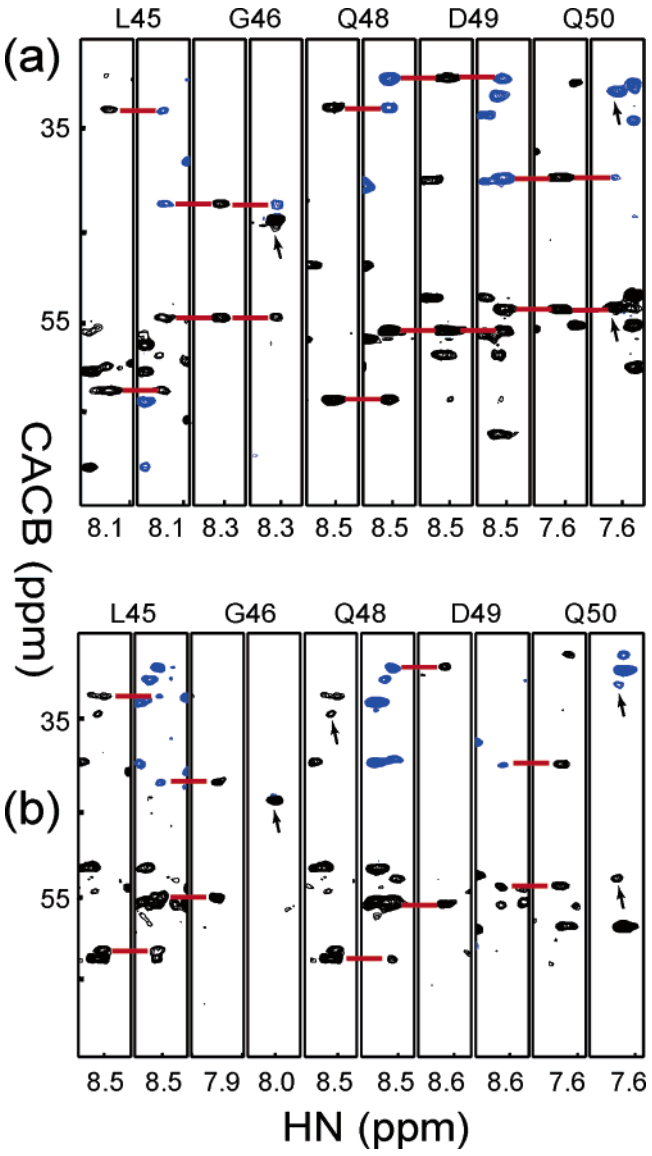

FIGURE 2: Strip plots of the 3D HNCACB and CBCA(CO)NH spectra of the binary complex HPPK•MgAMPCPP for residues P44−Q50 in loop 2. These residues have two sets of resonances as illustrated by panels (a) and (b). Each residue has two strips from different 2D planes of the CBCA(CO)NH (left) and HNCACB (right) data. Horizontal bars across the strips indicate the C^{α} and C^{β} connectivities between the residues. The arrows indicate the starting or ending residues of the connected fragments.

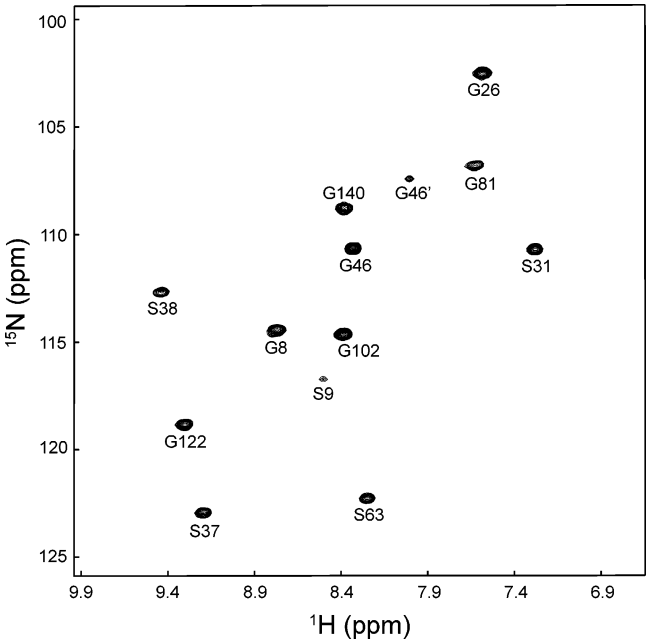

FIGURE 3: ^{1}H-^{15}N HSQC spectrum of the binary complex HPPK•MgAMPCPP. The protein was selectively labeled with ^{15}N-glycine/serine. Sequential assignments are labled with one-letter amino acid codes and residue numbers. The spectrum was recorded at 25 °C and a ^{1}H frequency of 600 MHz with coherence selection by pulsed field gradients and sensitivity enhancement.

lated, and the 20 structures with lowest energies and NOE violations are shown in Figure 4a. The NMR restraints and statistics of the structures are summarized in Table 1. As indicated by the RMSD values (Figure 5a, blue), the structures are well defined except for the three catalytic loops and the loop (residues 134−140) connected to the *C*-terminal short helix. As expected, the core structure consists of a central β-sheet and two helices on each side of the β-sheet (Figure 4b).

The high RMSD values of the residues in the three catalytic loops are undoubtedly due in part to the multiple conformations that these loops may assume, as indicated by the multiple sets of NMR signals and weak or missing NMR signals for many of the loop residues. However, the loops are not completely unrestrained or disordered. For example, even E87 in the middle of loop 3, which possesses one of the largest RMSD values in the ensemble of the 20 refined structures from the minimized mean structure, has one ambiguous and three unambiguous long-range NOE restraints, two medium range, six sequential, and seven intraresidue NOE restraints.

To further investigate the internal motions of these loops, heteronuclear {^{1}H}-^{15}N NOE data were acquired for the binary complex as shown in Figure 5b (blue). Heteronuclear {^{1}H}-^{15}N NOEs are sensitive to motions on the picosecond (ps)−nanosecond (ns) time scale (*27*−*32*). Overall, the protein is rather rigid with an average NOE of 0.80. However, loop 2 and the *C*-terminal region show significant motions on the ps−ns time scale. The NOE values of G46 in loop 2 and L155 in the *C*-terminal region are 0.22 and 0.39, respectively, among the lowest of all residues. Interestingly, although loop 3 certainly undergoes multiple conformational exchanges, its motion on the ps−ns time scale is not as prevalent as one would expect. Of the two measured residues in loop 3, one (R84) has a NOE of 0.58, which is significantly below average, and the other (E87) has a NOE of 0.88, which is above average. The two residues immediately adjacent to loop 3 also have high NOE values. G81 adjacent to the beginning of loop 3 has a NOE of 0.82, and T93 adjacent to the end of loop 3 has a NOE of 1.0, both above average. The incompleteness of the heteronuclear NOE data due to the missing or very weak signals, however, hinders the precise description of the loop 3 motion on the ps−ns time scale. Both the measured residue (N10) in loop 1 and the residue adjacent to loop 1 (G8) have NOE values that are above average, indicating that loop 1 is rigid on the ps−ns time scale, although this loop also undergoes conformational exchange on a slower time scale. The result suggested that the ps−ns conformational dynamics may be unrelated to the slower conformational exchanges as indicated by the multiple sets of peaks.

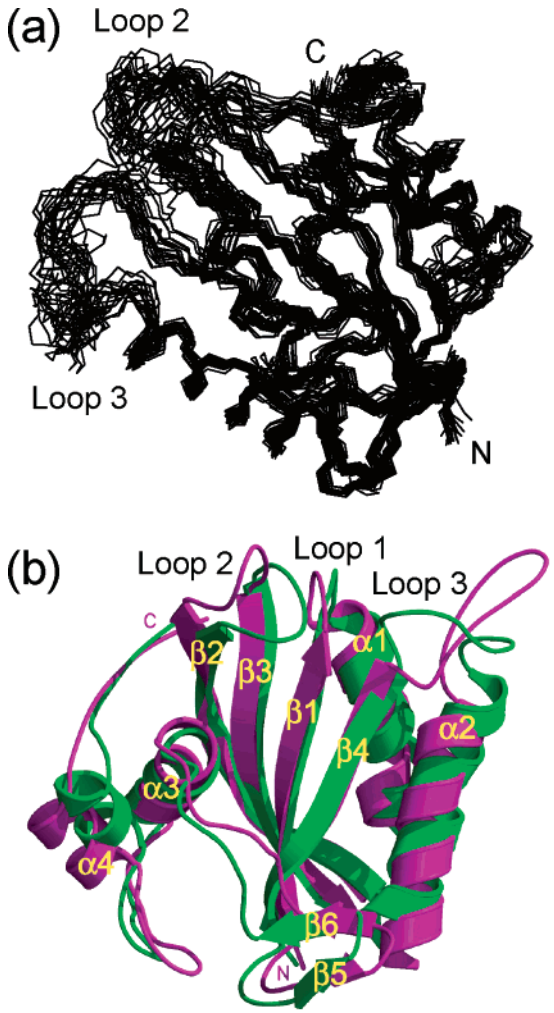

FIGURE 4: Ensemble of 20 NMR solution structures of the binary complex HPPK•MgAMPCPP (a) and its energy-minimized mean structure (green) superimposed with the energy-minimized mean NMR solution structure of the binary complex HPPK•MgAMPPCP (magenta) (b). The ribbon diagram was created with the programs Molscript (*40*) and Raster3D (*41*, *42*).

NMR Analysis of the Ternary Complex HPPK•MgAMPCPP•DMHP

Because the substrate HP tends to oxidize even in the presence of reducing agents such as DTT and tris(2-carboxyethyl)phosphine (TCEP), the substrate analogue DMHP (see Figure 1 for its chemical structure) was used in the NMR analysis of the ternary complex. In contrast to the binary complex HPPK•MgAMPCPP, the ^{1}H-^{15}N HSQC spectrum of the ternary complex HPPK•MgAMPCPP•DMHP showed not only excellent chemical shift dispersion but also uniformity in peak intensity (Figure 6). Although one residue in loop 1 and four residues in loop 3 were missing and many residues showed very weak cross-peaks in the ^{1}H-^{15}N HSQC spectrum of the binary complex, all of the backbone amide resonances in the three catalytic loops showed up in the ^{1}H-^{15}N HSQC spectrum of the ternary complex. The resonance assignment of the ternary complex was straightforward, as described in the Experimental Procedures section.

The solution structure determination of the ternary complex was achieved with iterative calculations using ARIA with an input file containing chemical shift assignments, dihedral restraints, and a list of NOE peaks. Twenty structures with lowest energies and minimal NOE violations were selected for structural analysis. The NOE restraints and statistics of the structures are also summarized in Table 1. An overlay of the C^{α} traces of the 20 solution structures is shown in Figure 7a. The solution structure of the ternary complex HPPK•MgAMPCPP•DMHP is very well defined, except for loop 3, which has an average RMSD of 1.6 Å for

Table 1: Statistics for the Ensembles of the Solution Structures of the Binary Complex HPPK•MgAMPCPP and the Ternary Complex HPPK•MgAMPCPP•DMHP

	binary complex	ternary complex
Structural restraints		
unambiguous NOEs[a]	3069	3557
ambiguous NOEs[a]	1204	1396
ϕ and ψ dihedral angles[b]	154	175
hydrogen bonds	47	none
Ensemble RMSD (Å)[c]		
secondary structure (backbone)	0.56 ± 0.049	0.44 ± 0.052
secondary structure (heavy)	1.12 ± 0.072	0.87 ± 0.075
all backbone	1.23± 0.16	0.70 ± 0.11
all heavy atoms	1.98 ± 0.16	1.32 ± 0.14
Average Violations per Structure		
NOEs and/or H-bonds	2.9	2.0
dihedrals	0.9	1.5
RMSD (Covalent Geometry)[c]		
bonds (Å)	0.0048 ± 0.0002	0.0046 ± 0.0003
angles (deg)	0.686 ± 0.045	0.661 ± 0.030
impropers (deg)	2.06 ± 0.15	1.88 ± 0.10
Ramachandran Space (%)[d]		
most favored region	67.8 ± 3.4	72.6 ± 2.8
additionally allowed	26.3 ± 3.3	21.4 ± 3.0
generously allowed	4.1 ± 1.7	4.5 ± 1.2
disallowed	1.8 ± 1.0	1.4 ± 0.8

[a] Obtained using Aria 1.2. [b] Obtained using TALOS. [c] Output by ARIA, calculated by CNS using the ensemble of 20 lowest energy structures. [d] Calculated with PROCHECK. The percentages are computed over all 20 lowest energy structures.

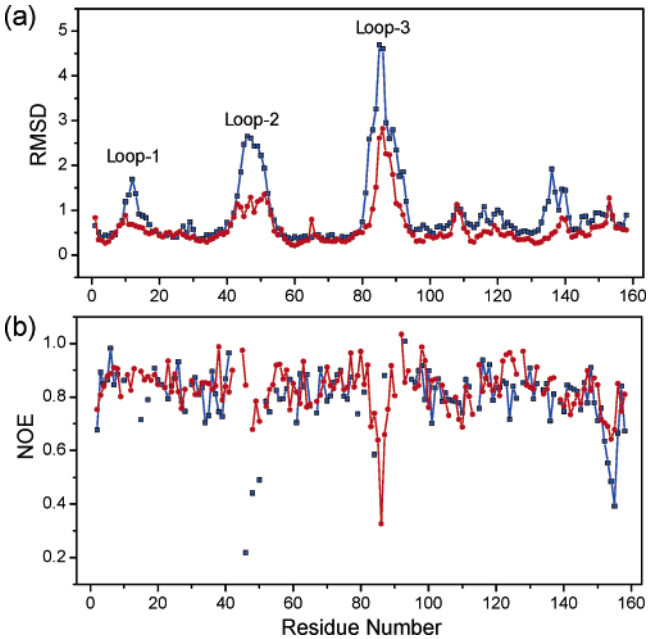

FIGURE 5: Backbone heavy atom RMSD (a) and {^{1}H}-^{15}N NOE (b) distributions of the binary complex HPPK•MgAMPCPP (blue) and the ternary complex HPPK•MgAMPCPP•DMHP (red). The RMSD values (Å) are the average of those of the ensemble of 20 refined solution structures of each complex from its energy-minimized mean structure.

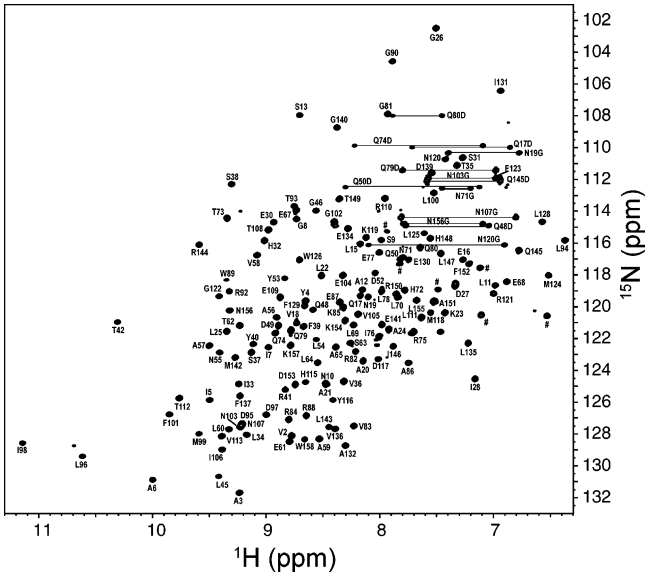

FIGURE 6: ^{1}H-^{15}N HSQC spectrum of the ternary complex HPPK•MgAMPCPP•DMHP recorded at 25 °C and a ^{1}H frequency of 600 MHz with coherence selection by pulsed field gradients and sensitivity enhancement. Sequential assignments are indicated with residue numbers.

the backbone heavy atoms (Figure 5a, red). The solution structure of the ternary complex HPPK•MgAMPCPP•DMHP is superimposed well with the crystal structure of the ternary complex HPPK•MgAMPCPP•HP (*3*). The differences are located in loops 2 and 3 (Figure 7b). The conformational differences between the two structures may be due to the use of the HP analogue DMHP. Similar conformation differences were also observed between the crystal structures of HPPK•MgAMPCPP•HP (*3*) and a ternary complex with an HP analogue (*14*).

In contrast to the binding of MgAMPCPP, the formation of the ternary complex by the binding of DMHP rigidifies the protein, as evidenced by the uniformity of the cross-peak intensities and the conversion of the multiple sets of NMR signals for the residues in loops 2 and 3 to a single set of NMR signals. To further investigate the internal motions of the ternary complex, heteronuclear {^{1}H}-^{15}N NOE data were acquired as shown in Figure 5b (red). The average of the {^{1}H}-^{15}N NOEs of the ternary complex was 0.83, indicating that the protein overall is rigid on the ps−ns time scale. In comparison with the binary complex, the core structure of the protein remains rigid, and loop 2 and the *C*-terminal region are rigidified. Interestingly, loop 3 remains mobile on the ps−ns time scale, with A86 in the middle of loop 3 having a {^{1}H}-^{15}N NOE value of only 0.33.

DISCUSSION

HPPK undergoes dramatic conformational changes during its catalytic cycle, and the conformational changes are important for catalysis. The enzyme has emerged as an excellent model for studying the role of protein dynamics in enzymatic catalysis. The major thrust of this work is to determine the solution structure of HPPK•MgAMPCPP, which is a better mimic of the binary substrate complex HPPK•MgATP, because MgAMPCPP is a better MgATP analogue for HPPK with respect to both structure and binding affinity. The structure of HPPK•MgATP is currently represented by that of HPPK•MgAMPPCP for the historic reasons as described in the Introduction section. The result of the present work revealed that the two binary complexes, HPPK•MgAMPCPP and HPPK•MgAMPPCP, have significantly different properties.

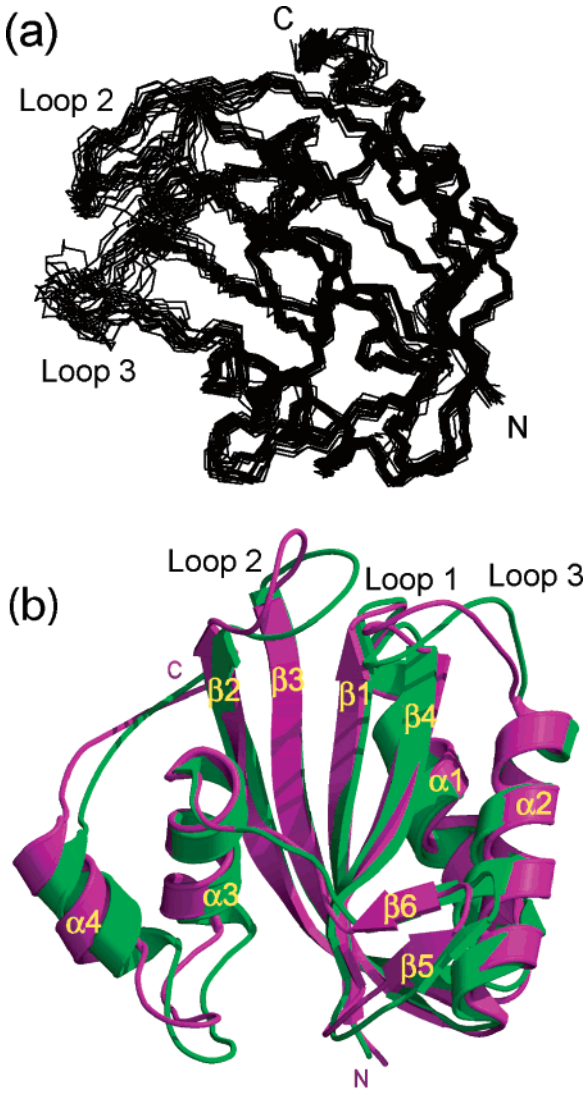

FIGURE 7: Ensemble of 20 NMR solution structures of the ternary complex HPPK•MgAMPCPP•DMHP (a) and its energy-minimized mean structure (green) superimposed with the crystal structure of the ternary complex HPPK•MgAMPCPP•HP (magenta) (b). The ribbon diagram was created with the programs Molscript (*40*) and Raster3D (*41*, *42*).

First, the NMR properties of HPPK•MgAMPPCP (a previous study (*4*, *8*)) and HPPK•MgAMPCPP (this work) are quite different. Specifically, the ^{1}H-^{15}N HSQC spectrum of HPPK•MgAMPCPP showed two sets of cross-peaks for some residues and missing or very weak cross-peaks for others in the catalytic loops, but only one set of cross-peaks was found for HPPK•MgAMPCPP. The results suggest that the catalytic loops of HPPK•MgAMPCPP undergo slow conformational exchange on the NMR chemical shift time scale, but those of HPPK•MgAMPCPP do not show such a conformational exchange. Second, loops 2 and 3 assume quite different conformations in the two binary complexes (Figures 4b and S2). Considering that the binary complex HPPK•MgAMPCPP can assume multiple conformations, a

minimized mean structure may be too simplistic to represent the conformations of this binary complex. Therefore, we also performed a pairwise comparison of the ensemble of the conformers of HPPK•MgAMPCPP with that of HPPK•MgAMPPCP, and found that loops 2 and 3 assume different conformations in the two binary complexes (Figure S3). Because the NMR properties and conformations of the two binary complexes HPPK•MgAMPCPP and HPPK•MgAMPPCP are significantly different (this work) and MgAMPCPP is a better MgATP analogue for HPPK (*3*, *11*, *14*), we suggest that the conformational properties of the binary substrate complex HPPK•MgATP be represented by HPPK•MgAMPCPP rather than by HPPK•MgAMPPCP.

Atomic structures are available for nearly every stage of the catalytic cycle of *E. coli* HPPK (*3*−*5*, *12*, 14). The structures of the various complexes have been obtained with substrates, products, and their analogues, mostly by X-ray crystallography. The conformational transitions during the catalytic cycle can be described by an induced fit model, that is, one conformation to another. The present work, along with the previous NMR study (*8*), however, supports a model for the conformational transitions that involve multiple conformation equilibria as described below.

First, the catalytic loops of the apo enzyme possess multiple conformations. The crystal structure of the apo enzyme reveals two conformations for loop 1 (*12*). Furthermore, 16 residues showed no cross-peaks or very weak ones in the ^{1}H-^{15}N HSQC spectrum of the apo enzyme (*8*). Seven of these residues are located in the catalytic loops, Q48 in loop 2 and R82, V83, A86, W89, G90 and R92 in loop 3, and six residues, E77-Q80, T93, D95, and L96, are in the vicinities of loop 3, suggesting that both loops 2 and 3 assume multiples conformations exchanging on the intermediate NMR chemical shift time scale. Second, the results of this work indicate that the binary substrate complex of HPPK can assume multiple conformations on the slow NMR chemical shift time scale, as evidenced by multiple sets of NMR signals for several residues in loops 2 and 3 and the very weak or missing NH cross-peaks for several residues in loops 1 and 3. Third, the ternary complex shows only one set of NMR signals, and the cross-peak intensities are rather uniform, suggesting that the binding of the second substrate shifts the multiple conformations of the binary complex to an apparently single conformation of the ternary complex. The ternary complex is also rigid on the ps−ns time scale, except for loop 3, which remains mobile on the ps−ns time scale.

Therefore, it is quite possible that the apo HPPK assumes a range of conformations. Some of the conformations become more populated upon the binding of the first substrate, as evidenced by the multiple sets of NMR signals for the loop 2 and loop 3 residues in the binary complex HPPK•MgAMPCPP. It is unlikely that the same ligand, MgAMPCPP, induces several different conformations; rather, MgAMPCPP may form complexes with several different preexisting conformers. Although the binary complex is still flexible, the binding of the first substrate partially rigidifies HPPK to a narrower range of conformations undergoing slower conformational exchange. Thus, a redistribution of conformational populations occurs in the formation of the binary complex, although not just a single conformer is selected. The multiple conformational equilibria shift to an apparently single conformation after the binding of HP.

There are two types of general models that have been proposed for conformational transitions associated with ligand binding, the classical induced fit model (*33*, *34*) and the more recent population shift or selected fit model (*35*−*39*). Unlike a lock-and-key model, which presumes a rigid protein molecule, both the induced fit and population shift models agree that protein molecules are flexible (*33*−*37*). However, the induced fit model presumes that a protein assumes an apo conformation prior to ligand binding and changes to a bound conformation only after ligand binding (*33*, *34*). In contrast, the population shift model presumes that the apo protein assumes multiple conformations and that ligand binding shifts the multiple conformational equilibria in favor of one conformation (*35*−*37*). The major difference between the two models is that in the induced fit model, the conformation of the complex does not exist prior to ligand binding, and the bound conformation is induced by the ligand binding, whereas in the population shift model, the conformation of the complex is one of the conformations that a protein can assume in the absence of the ligand, and ligand binding only shifts the conformational equilibria to that of the bound form.

Because the apo enzyme and the binary substrate complex both assume multiple conformations, the conformational transitions in HPPK cannot be described by the classical induced fit model of one conformation to another. The conformational transitions do exhibit features of the population shift model, but it is not certain whether the conformations of the ligand-bound forms exist in the absence of the ligands because the solution conformations of the apo enzyme have not been determined, and the solution conformations of the binary complex HPPK•MgAMPCPP reported in this work are only those of the predominant species. The conformation of the ternary complex is probably not a preexisting one because both the MgATP and HP binding sites are sealed and inaccessible to the two substrates. In other words, the conformation of the ternary substrate complex is induced by the binding of HP to the binary substrate complex HPPK•MgATP. Furthermore, the hydrogen bond network that couples the three catalytic loops may play a critical role in the conformational transitions (*3*). In this sense, the conformational transitions in HPPK are best described by the combined features of the population shift and induced fit models.

HPPK catalyzes a two substrate reaction, and the reaction takes place only after the formation of the ternary substrate complex. The kinetic mechanism of the HPPK-catalyzed reaction is an ordered one with MgATP binding to the enzyme first (*10*, *11*). The fact HP cannot form a stable binary complex with HPPK is not because the HP binding site is blocked (*12*). It is probably because the conformational transition required for the population shift cannot occur without the binding of the first substrate MgATP. Rather than shifting the multiple conformational equilibria to a single conformation, the binding of the first substrate only alters the dynamics of the enzyme to facilitate the binding of the second substrate HP to form the ternary complex. The structure of the binary complex is, thus, best represented by an ensemble of conformations.

ACKNOWLEDGMENT

We thank Mr. Kermit Johnson and Dr. Aizhuo Liu for NMR instrumentation and Dr. Stepan Sklenak for computational support.

SUPPORTING INFORMATION AVAILABLE

Scheme showing the route for the chemical synthesis of DMHP and Figures showing two sets of cross-peaks for A86 and E87, the RMSDs of various structural comparisons, and the superposition of the NMR ensembles of conformers of the binary complexes HPPK•MgAMPCPP and HPPK•MgAMPPCP. This material is available free of charge via the Internet at http://pubs.acs.org.

REFERENCES

1. Bermingham, A., and Derrick, J. P. (2002) The folic acid biosynthesis pathway in bacteria: evaluation of potential for antibacterial drug discovery, *BioEssays 24*, 637−648.
2. Blakley, R. L., and Benkovic, S. J. (1984) *Folates and Pterins*, John Wiley & Sons, New York.
3. Blaszczyk, J., Shi, G., Yan, H., and Ji, X. (2000) Catalytic center assembly of HPPK as revealed by the crystal structure of a ternary complex at 1.25 Å resolution, *Structure 8*, 1049−1058.
4. Xiao, B., Shi, G., Gao, J., Blaszczyk, J., Liu, Q., Ji, X., and Yan, H. (2001) Unusual conformational changes in 6-hydroxymethyl-7,8-dihydropterin pyrophosphokinase as revealed by X-ray crystallography and NMR, *J. Biol. Chem. 276*, 40274−40281.
5. Blaszczyk, J., Shi, G., Li, Y., Yan, H., and Ji, X. H. (2004) Reaction trajectory of pyrophosphoryl transfer catalyzed by 6-hydroxymethyl-7,8-dihydropterin pyrophosphokinase, *Structure 12*, 467−475.
6. Blaszczyk, J., Li, Y., Wu, Y., Shi, G., Ji, X. H., and Yan, H. (2004) Essential roles of a dynamic loop in the catalysis of 6-hydroxymethyl-7,8-dihydropterin pyrophosphokinase, *Biochemistry 43*, 1469−1477.
7. Li, Y., Blaszczyk, J., Wu, Y., Shi, G. B., Ji, X. H., and Yan, H. G. (2005) Is the critical role of loop 3 of *Escherichia coli* 6-hydroxymethyl-7,8-dihydropterin pyrophosphokinase in catalysis due to loop-3 residues arginine-84 and tryptophan-89? Site-directed mutagenesis, biochemical, and crystallographic studies, *Biochemistry 44*, 8590−8599.
8. Shi, G., Gao, J., and Yan, H. (1999) ^{1}H, ^{13}C and ^{15}N resonance assignments of *Escherichia coli* 6-hydroxymethyl-7,8-dihydropterin pyrophosphokinase and its complex with MgAMPPCP, *J. Biomol. NMR 14*, 189−190.
9. Yang, R., Lee, M. C., Yan, H. G., and Duan, Y. (2005) Loop conformation and dynamics of the *Escherichia coli* HPPK apo-enzyme and its binary complex with MgATP, *Biophys. J. 89*, 95−106.
10. Bermingham, A., Bottomley, J. R., Primrose, W. U., and Derrick, J. P. (2000) Equilibrium and kinetic studies of substrate binding to 6-hydroxymethyl-7,8-dihydropterin pyrophosphokinase from *Escherichia coli*, *J. Biol. Chem. 275*, 17962−17967.
11. Li, Y., Gong, Y., Shi, G., Blaszczyk, J., Ji, X., and Yan, H. (2002) Chemical transformation is not rate-limiting in the reaction catalyzed by *Escherichia coli* 6-hydroxymethyl-7,8-dihydropterin pyrophosphokinase, *Biochemistry 41*, 8777−8783.
12. Xiao, B., Shi, G. B., Chen, X., Yan, H. G., and Ji, X. H. (1999) Crystal structure of 6-hydroxymethyl-7,8-dihydropterin pyrophosphokinase, a potential target for the development of novel antimicrobial agents, *Structure 7*, 489−496.
13. Hennig, M., Dale, G. E., D'Arcy, A., Danel, F., Fischer, S., Gray, C. P., Jolidon, S., Muller, F., Page, M. G. P., Pattison, P., and Oefner, C. (1999) The structure and function of the 6-hydroxymethyl-7,8-dihydropterin pyrophosphokinase from Haemophilus influenzae, *J. Mol. Biol. 287*, 211−219.
14. Stammers, D. K., Achari, A., Somers, D. O., Bryant, P. K., Rosemond, J., Scott, D. L., and Champness, J. N. (1999) 2.0 Å X-ray structure of the ternary complex of 7,8-dihydro-6-hydroxymethylpterin pyrophosphokinase from *Escherichia coli* with ATP and a substrate analogue, *FEBS Lett. 456*, 49−53.
15. Wood, H. C. S., and Stuart, A. Pteridine derivatives useful as bacteriostats. S. African Patent 7000576, 1970.
16. Boon, W. R., and Jones, W. G. M. (1951) Specific inhibitors in vitamin biosynthesis. Part 7. Syntheses of blocked 7,8-dihydropteridines via α-amino ketones, *J. Chem. Soc. B*, 596.
17. Al-Hassan, S. S., Cameron, R. J., Curran, A. W. C., Lyall, W. J. S., Nicholson, S. H., Robinson, D. R., Stuart, A., Suckling, C. J., Stirling, I., and Wood, H. C. S. (1985) Specific inhibitors in vitamin biosynthesis. Part 7. Synthesis of blocked 7,8-dihydropteridine via α-amino ketones, *J. Chem. Soc., Perkin Trans. 1*, 1645−1659.
18. De Jong, R. L., Davidson, J. G., Dozeman, G. J., Fiore, P. J., Giri, P., Kelly, M. E., Puls, T. P., and Seamans, R. E. (2001) The chemical development of CI-972 and CI-1000: A continuous nitration, a $MgCl_2/Et_3N$-mediated C-alkylation of a chloronitropyrimidine, a catalytic protodediazotization of a diazonium salt, and an air oxidation of an amine, *Org. Process Res. Dev. 5*, 216−225.
19. Delaglio, F., Grzesiek, S., Vuister, G. W., Zhu, G., Pfeifer, J., and Bax, A. (1995) NMRPipe: a multidimensional spectral processing system based on UNIX pipes, *J. Biomol. NMR 6*, 277−293.
20. Johnson, B. A., and Blevins, R. A. (1994) NMRView: A computer program for the visualization and analysis of NMR data, *J. Biomol. NMR 4*, 603−614.
21. Farrow, N. A., Muhandiram, R., Singer, A. U., Pascal, S. M., Kay, C. M., Gish, G., Shoelson, S. E., Pawson, T., Forman Kay, J. D., and Kay, L. E. (1994) Backbone dynamics of a free and phosphopeptide-complexed *src* homology 2 domain studied by ^{15}N NMR relaxation, *Biochemistry 33*, 5984−6003.
22. Linge, J. P., O'Donoghue, S. I., and Nilges, M. (2001) Automated assignment of ambiguous nuclear overhauser effects with ARIA, *Methods Enzymol. 339*, 71−90.
23. Linge, J. P., Habeck, M., Rieping, W., and Nilges, M. (2003) ARIA: automated NOE assignment and NMR structure calculation, *Bioinformatics 19*, 315−316.
24. Linge, J. P., Williams, M. A., Spronk, C., Bonvin, A., and Nilges, M. (2003) Refinement of protein structures in explicit solvent, *Proteins: Struct., Funct., Genet. 50*, 496−506.
25. Brünger, A. T., Adams, P. D., Clore, G. M., DeLano, W. L., Gros, P., Grosse-Kunstleve, R. W., Jiang, J.-S., Kuszewski, J., Nilges, N., Pannu, N. S., Read, R. J., Rice, L. M., Simonson, T., and Warren, G. L. (1998) Crystallography and NMR system (CNS): A new software system for macromolecular structure determination, *Acta Crystallogr., Sect D 54*, 905−921.
26. Cornilescu, G., Delaglio, F., and Bax, A. (1999) Protein backbone angle restraints from searching a database for chemical shift and sequence homology, *J. Biomol. NMR 13*, 289−302.
27. Kay, L. E. (1998) Protein dynamics from NMR, *Nat. Struct. Biol. 5*, 513−517.
28. Ishima, R., and Torchia, D. A. (2000) Protein dynamics from NMR, *Nat. Struct. Biol. 7*, 740−743.
29. Palmer, A. G. (2004) NMR characterization of the dynamics of biomacromolecules, *Chem. Rev. 104*, 3623−3640.
30. Atkinson, R. A., and Kieffer, B. (2004) The role of protein motions in molecular recognition: insights from heteronuclear NMR relaxation measurements, *Prog. Nucl. Magn. Reson. Spectrosc. 44*, 141−187.
31. Kay, L. E. (2005) NMR studies of protein structure and dynamics, *J. Magn. Reson. 173*, 193−207.
32. Jarymowycz, V. A., and Stone, M. J. (2006) Fast time scale dynamics of protein backbones: NMR relaxation methods, applications, and functional consequences, *Chem. Rev. 106*, 1624−1671.
33. Koshland, D. E. J. (1958) Application of a theory of enzyme specificity to protein synthesis, *Proc. Natl. Acad. Sci. U.S.A. 44*, 98−123.
34. Koshland, D. E. (1994) The key-lock theory and the induced fit theory, *Angew. Chem., Int. Ed. Engl. 33*, 2375−2378.
35. Kumar, S., Ma, B., Tsai, C. J., Sinha, N., and Nussinov, R. (2000) Folding and binding cascades: dynamic landscapes and population shifts, *Protein Sci. 9*, 10−19.
36. Tsai, C. J., Kumar, S., Ma, B. Y., and Nussinov, R. (1999) Folding funnels, binding funnels, and protein function, *Protein Sci. 8*, 1181−1190.
37. Tsai, C. J., Ma, B. Y., Sham, Y. Y., Kumar, S., and Nussinov, R. (2001) Structured disorder and conformational selection, *Proteins 44*, 418−427.
38. Kern, D., and Zuiderweg, E. R. P. (2003) The role of dynamics in allosteric regulation, *Curr. Opin. Struct. Biol. 13*, 748−757.

39. Formaneck, M. S., Ma, L., and Cui, Q. (2006) Reconciling the "old" and "new" views of protein allostery: A molecular simulation study of chemotaxis Y protein (CheY), *Proteins 63*, 846−867.
40. Kraulis, P. J. (1991) MOLSCRIPT: a program to produce both detailed and schematic plots of protein structures, *J. Appl. Crystallogr. 24*, 946−950.
41. Bacon, D. J., and Anderson, W. F. (1988) A fast algorithm for rendering space-filling molecule pictures, *J. Mol. Graphics 6*, 219−220.
42. Merritt, E. A., and Bacon, D. J. (1997) Raster3D: Photorealistic molecular graphics, *Methods Enzymol. 277*, 505−524.

BI061057M